Journal Pre-proof

D816V KIT mutation induces mitochondrial morphologic and functional changes through BNIP3 downregulation in human myeloid cell lines ROSA and TF-1.

S Cisa-Wieczorek , MI Hernández-Alvarez , M Parreño , JP Muñoz , E Bussaglia , M Carricondo , J Ubeda , P Dubreuil , A Zorzano , F Brenet , JF Nomdedeu

PII: S0301-472X(25)00039-6
DOI: https://doi.org/10.1016/j.exphem.2025.104748
Reference: EXPHEM 104748

To appear in: *Experimental Hematology*

Received date: 9 July 2024
Revised date: 5 February 2025
Accepted date: 12 February 2025

Please cite this article as: S Cisa-Wieczorek , MI Hernández-Alvarez , M Parreño , JP Muñoz , E Bussaglia , M Carricondo , J Ubeda , P Dubreuil , A Zorzano , F Brenet , JF Nomdedeu , D816V KIT mutation induces mitochondrial morphologic and functional changes through BNIP3 down-regulation in human myeloid cell lines ROSA and TF-1., *Experimental Hematology* (2025), doi: https://doi.org/10.1016/j.exphem.2025.104748

Highlights

- Cell lines with the KIT D816V mutation exhibit elevated oxidative phosphorylation.
- KIT D816V mutation increases the mitochondrial number and SOX production.
- KIT D816V shows infra expression of the BNIP3 mitophagy marker.
- Patients with AML and KIT D816V mutation express lower levels of BNIP3.

D816V *KIT* mutation induces mitochondrial morphologic and functional changes through BNIP3 downregulation in human myeloid cell lines ROSA and TF-1.

Short title: *KIT* D816V effects on mitochondrial number and activity

Authors: Cisa-Wieczorek S[1], Hernández-Alvarez MI [2,3], Parreño M[4], Muñoz JP[2,5,6], Bussaglia E[1], Carricondo M[1], Ubeda J[1], Dubreuil P[7], Zorzano A[2,5,6], Brenet F[7], Nomdedeu JF*

Short title: KIT D816V effects on mitochondrial number and activity

A

Corresponding author*: Josep F. Nomdedeu
Laboratori d´Hematologia. Servei d´Hematologia.
Hospital de la Santa Creu i Sant Pau
Universitat de Barcelona/IIB Sant Pau
Sant Quintí, 89. 08041 Barcelona. SPAIN

Other affiliations:

[1]Laboratory of Hematology, Department of Hematology. Hospital de la Santa Creu i Sant Pau. Universitat Autònoma de Barcelona/IIB Sant Pau, Spain.

[2]Departament de Bioquímica i Biomedicina Molecular, Universitat de Barcelona, Barcelona, Spain.

[3]CIBER de Diabetes y Enfermedades Metabólicas Asociadas (CIBERDEM), Madrid, Spain.

[4]Translational Molecular Oncology, IIB-Sant Pau, Hospital de la Santa Creu i Sant Pau (HSCSP), Barcelona, Spain.

[5]Centro de Investigación Biomédica en Red de Diabetes y Enfermedades Metabólicas Asociadas (CIBERDEM), Instituto de Salud Carlos III, Madrid, Spain.

[6]Institute for Research in Biomedicine (IRB Barcelona), The Barcelona Institute of Science and Technology, Barcelona, Spain.

[7]Centre de Recherche en Cancérologie de Marseille (CRCM), INSERM U1068, UMR7258 CNRS, Aix-Marseille Université, Institut Paoli-Calmettes, Marseille, France.

Abstract word count:194

Main document word count: 3657
Reference count:50
Figure count:5

ABSTRACT

The KIT receptor is a transmembrane protein found on the surface of many different cell types. Mutant forms of KIT are drivers of myeloid neoplasms, including systemic mastocytosis. The KIT D816V mutation is the most common, leading to constitutive activation of the receptor and its downstream targets, and it is highly resistant to c-KIT inhibitors. Metabolic rewiring is a common trait in cancer. We analyzed the metabolic profile induced by *the* KIT D816 mutation, measuring mitochondrial parameters in two myeloid cell lines. We found that *the* KIT D816V mutation causes

a significant increase in mitochondrial abundance and activity associated with superoxide production, which could promote DNA instability. Functional and morphological changes in mitochondria were associated with reduced levels of BNIP3 protein expression. We also detected low BNIP3 levels in clinical acute myeloid leukemia samples harboring D816V mutations. In addition, we have found a constitutive mTOR activation in mutated cells, a pathway that has been shown to regulate autophagy.

Our data suggest that *KIT* D816V increases mitochondrial activity through BNIP3 down expression, which increases mitochondrial number through the autophagy pathway. Alterations in the cellular metabolism induced by *the* KIT D816V mutation could be therapeutically exploited.

Keywords: Myeloid neoplasm, C-KIT D816V, autophagy.

Highlights

- Cell lines with the KIT D816V mutation exhibit elevated oxidative phosphorylation.
- KIT D816V mutation increases the mitochondrial number and SOX production.
- KIT D816V shows infra expression of the BNIP3 mitophagy marker.
- Patients with AML and KIT D816V mutation express lower levels of BNIP3.

INTRODUCTION

The c-kit receptor (proto-oncogene receptor tyrosine kinase), CD117, is a transmembrane protein with tyrosine kinase activity encoded by the oncogene KIT. KIT is a member of the type III receptor tyrosine kinase family. Binding the KIT-specific ligand, stem cell factor (SCF), to the KIT receptor induces its dimerization, intermolecular auto-phosphorylation of specific tyrosine residues, and protein tyrosine kinase activation. Consequently, through KIT receptor activation, SCF triggers specific intracellular signaling pathways that promote

proliferation, migration, survival, and differentiation of hematopoietic progenitors, melanocytes, and germ cells [1].

KIT mutations have been found in mastocytosis [2], acute myeloid leukemia (AML) [3], gastrointestinal stromal tumors (GISTs) [4], melanoma [5], and germ cell tumors [6]. D816V is the most common KIT allele. It is localized in the activation loop of the kinase domain and causes constitutive ligand-independent activation in the absence of SCF, conferring growth capacities to hematopoietic cells. The KIT D816V mutation produces a constitutive phosphorylation of the receptor and of its downstream effectors, AKT, ERK, and STAT5 [7, 8].

Pharmacologic c-Kit inhibitors have been developed, but they only effectively block wild-type and juxtamembrane mutations. Substitution of aspartate (D) to valine (V) at position 816, located in the active loop of the intracellular enzymatic pocket, is highly resistant to c-Kit inhibitors [9].

Altered metabolism is a hallmark of cancer [10], and many studies have suggested that oncogenes induce metabolic alterations [11], as the Warburg effect describing a switch to glycolysis from oxidative phosphorylation (OXPHOS) has been associated with many cancers. However, mitochondrial functional studies have also shown that this metabolic pattern is not present in every cancer and that some tumors rely on OXPHOS for growth.

Through the formation of the autophagosomes, double-membrane vesicles, cells may capture their own organelles or cytoplasm, which are subsequently degraded in lysosomes through autophagy. The resulting breakdown products can support metabolism. The pro-apoptotic BH3-only protein BNIP3 is a potent inducer of mitochondrial autophagy. To target the mitochondria for autophagosome clearance, BNIP3 is tethered to the outer membrane of the mitochondria. The mechanistic link between the proto-oncogene KIT and cellular metabolism, including autophagy, remains unknown.

In order to identify novel targets for myeloid malignancies, this work aims to examine the metabolic profile linked to the KIT D816V mutation in myeloid cells. We employed two human cell lines for this aim: the erythroleukemia cell line TF-1 [12] and the mast cell line (MC) ROSA [13]. We compared wild-type (KIT WT) versions of these cell lines with those bearing the KIT D816V mutation that converts both cell lines into SCF-independent cells. Preliminary research employing human AML samples has confirmed the results obtained in cell lines.

RESULTS

Respiratory rates and capacity in KIT D816V cells

To study the respiratory rates of the D816V mutation, we used ROSA and TF-1 WT cells and their mutated KIT versions. Using a Seahorse XF24 extracellular flux analyzer, we detected a significant increase in mitochondrial respiration in both mutated cell lines compared to KIT WT cells (Figure 1A, B). Before the addition of complex inhibitors, the oxygen consumption rate (OCR) was measured, and basal mitochondrial respiration was calculated, subtracting these values from those of non-mitochondrial respiration (Figure 1C, D). The cells harboring the KIT mutation in baseline conditions have greater energetic production. OCR increases by 40% in ROSA KIT D816V and 30% in TF-1 KIT D816V. After basal respiration measurements, oligomycin was injected into the wells. Oligomycin is a specific inhibitor of ATPase activity that prevents electron transport. It produces a reduction in OCR according to the portion of oxygen that is being used for ATP production (ATP-linked production). We observed that ROSA KIT D816V and TF-1 KIT D816V cells consumed more than 100 pmol/min of OCR to produce ATP compared with KIT WT cells (Figure 1C, D). These results suggest that the basal respiration portion used to create ATP is higher in KIT-mutated cells.

Oligomycin injection also allowed us to calculate proton leak, a measure of oxygen consumption not coupled to ATP production. The increased proton leak value could indicate mitochondrial dysfunction, but no significant differences were obtained in our experiments (Supplementary Figure 1A, 1C).

CCCP, a mitochondrial membrane uncoupler, was injected into the Seahorse medium to analyze the maximal mitochondrial respiratory capacity. CCCP mimics physiological maximal oxygen consumption that can reach cells under stress conditions. ROSA KIT D816V had a value of maximal respiratory capacity 60% greater than ROSA KIT WT cells, whereas TF-1 KIT D816V doubled it compared to WT cells (Figure 1C,D) . We noticed a relatively low maximal capacity of the TF-1 cell line, which could be explained by the fact that these cells are from a patient with AML, and it is shown that AML cells have a low spare reserve capacity [14]. However, ROSA maximal respiratory capacity was more evident; MC degranulation requires mitochondrial fission and translocation to the cell surface, which could require a high mitochondrial reserve capacity [15].

Tetramethylrhodamine, methyl ester (TMRM), is a cell-permeant dye that accumulates in active and healthy mitochondria. Mitochondrial membrane potential (Δψm) increases with TMRM fluorescence, whereas declining mitochondrial function or inactive mitochondria are typically associated with a fluorescence intensity reduction. We used TMRM to measure Δψm, and consistent with our OCR data results, we found that ROSA and TF-1 KIT mutated cells had greater fluorescence signals of 80% and 70%, respectively, compared to those obtained in KIT WT cells (Figure 1E, F) These results suggest that KIT D816V cell lines had

higher mitochondrial activity. Still, this increased value could result from increased mitochondrial number or activity.

Warburg's theory of cancer suggests that insufficient cellular respiration could be caused by mitochondrial impairment [16, 17]. Our Seahorse experiments did not show a defect in mitochondrial function, but rather the opposite. To confirm that KIT D816V cells did not have a glycolytic phenotype characterized by increased glucose consumption, we measured glucose uptake by flow cytometry using 2-NBDG, a fluorescent tracer analog to glucose. As expected, according to our previous results, the KIT D816V mutation did not produce a switch to glycolysis because the levels of glucose uptake did not show differences between KIT WT and KIT D816V cells (Figure 1G, H).

Next, we determined if the increase in the observed mitochondrial activity was also associated with higher ATP production. We measured the ATP content using a quantitative bioluminescence assay. We observed a two-fold increase in ATP production in TF-1 KIT D816V and a five-fold increase in ROSA KIT D816V compared to WT cells (Figure 1E, J).

Taking all these results together, we conclude that the KIT D816V mutation increases mitochondrial OCR, including basal, ATP-linked, and maximal respiration and ATP production.

D816V mutation and mitochondrial superoxide levels

Oxygen consumed by mitochondria is reduced to water in the terminal reaction of the respiratory chain by cytochrome C oxidase. A portion of the oxygen consumed is converted to a superoxide anion as a byproduct of the mitochondrial respiratory chain [18]. We found that superoxide production was five times greater in ROSA mutated cells, and for TF-1 mutated cells, we obtained a value 50% greater than KIT WT cells (Figure 2A, B). KIT D816V cells disclosed a significant increase in superoxide production that could be attributed to the increased mitochondrial function. To confirm that the higher superoxide level observed was a consequence of mitochondrial metabolism and was not produced by superoxide scavenger upregulation, we measured the mitochondrial superoxide dismutase enzyme (SOD2) levels located in the mitochondrial matrix by western blot. SOD2 catalyzes the dismutation of O2- into molecular oxygen and hydrogen peroxide (H2O2) and decreases O2- a level that damages cells at excessive concentrations. We observed that SOD2 protein levels were the same in WT and KIT D816V cells (Figure 2E), confirming that O2- levels rose by increasing mitochondrial activity and not by uneven enzymatic activity.

To further analyze whether the superoxide affected oxidative stress, we analyzed 8-OHdG, a DNA damage marker. Cells were stained with 8-OHG and DAPI for quantification and

visualized by confocal fluorescence microscopy (Figure 2C) to quantify the punctate (Figure 2D). We found that punctate 8-OHdG in mutated ROSA cells is bigger and increases in number.

In sharp contrast, the 8-OHG signal does not have significant differences between TF-1 KIT WT and D816V cells. It is found that there is a very high level of 8-OHG in WT cells (Supplementary Figure 2). It could be a consequence of the highly rearranged hyperdiploid karyotype and mutations.

We concluded that increased mitochondrial activity in ROSA KIT D816V cells was associated with higher O2- production and, therefore, a higher rate of oxidative damage.

Mitochondria in KIT mutated cells

Next, we assessed the mitochondrial copy DNA number by measuring mitochondrial DNA (mtDNA) by Q-PCR. The mtDNA copy number was significantly higher in ROSA and TF-1 cells carrying the KIT D816V mutation (Figure 3A, B). Under these conditions, we also detected an enhanced abundance of mitochondrial complex V-ATP5A in KIT mutant cells (Figure 3F).

We analyzed the ultrastructural features of ROSA and TF-1 mitochondria by transmission electron microscopy (TEM) (Figure 3C). We observed that cells harboring the KIT mutation have more mitochondria (Figure 3D, E), but they appear smaller than those from KIT WT cells; indeed, the form is round compared to WT cells with the mitochondria elongated. In both cases, mitochondria are homogeneously distributed into the cytoplasm.

To assess the size of mitochondria, we calculated the mitochondrial area, and we found that the mitochondria of KIT D816V ROSA and TF-1 cells were significantly smaller compared to those of KIT WT cells (Figure 3G, H).

Autophagy in KIT mutated cell lines.

Increased mitochondrial number could be a consequence of increased mitochondrial biogenesis or decreased degradation, a process called mitophagy. We examined whether the difference in mitochondrial number in cells carrying the KIT mutation was due to mitochondrial biogenesis upregulation. We analyzed the expression of critical activators of mitochondrial biogenesis, but we found no differences in their expression (Supplementary Figure 3).

To test if altered mitophagy could explain the mitochondrial changes observed in KIT mutated cells, we analyzed the mitophagy marker BNIP3 (a pro-apoptotic BH3-only protein subfamily) and the levels of autophagosome-localized LC3 (Microtubule-associated Protein 1 Light Chain 3), a specific marker for autophagy.

We observed small but significantly reduced levels of BNIP3 in ROSA and TF-1 mutated cells compared to WT cells (Figure 4A). When autophagy is activated, a cytosolic form of LC3 (LC3-I) is conjugated to phosphatidylethanolamine to form LC3-phosphatidylethanolamine conjugate (LC3-II) [19]. We observed that LC3-II is reduced in ROSA-mutated cells, indicating that autophagy is reduced compared to its wild-type version. However, we haven't found differences in TF-1 cells.

We analyzed BNIP3 expression by Q-PCR and observed, as in the immunoblotting analysis, a decreased level of BNIP3 in mutated KIT cells (Figure 4B).

We treated cells with Bafilomycin A1, an autophagic inhibitor that prevents the maturation of autophagic vacuoles and results in the accumulation of autophagosomes. These accumulated autophagosomes showed an increased expression of LC3-II that can be measured. For this purpose, we treated ROSA cells with Bafilomycin A1 for 6 hours at 100 nM and TF-1 for 7 hours at 130 nM. In these conditions, we confirmed that autophagy is reduced in ROSA D816V cells (Figure 4C), and we observed that mutated TF-1 cells treated with Bafilomycin had decreased LC3-II, I indicating a decrease in the formation of autophagosomes. Indeed, BNIP3 levels in KIT WT cells were higher compared to KIT D816V cells in both cases (Figure 4C). Altogether, these data indicate that autophagy is decreased in mutated KIT cells.

Given these results, we overexpressed BNIP3 in KIT D816V to ensure that BNIP3 controls autophagy. We infected KIT D816V cells with the BNIP3 adenovirus (BNIP3 ORF). As expected, BNIP3 upregulation was associated with an increased level of LC3-II (Figure 4D).

Moreover, to analyze if BNIP3 was responsible for the increased mitochondrial abundance in KIT D816V cells, we quantified the mtDNA in cells infected with BNIP3. Overexpression of BNIP3 induced a decline in mtDNA in both ROSA and TF-1 D816V cell lines, reverting the mutated phenotype (Figure 4E). We conclude that BNIP3 expression increases autophagy and controls mitochondrial number in our myeloid models.

The kinase mTOR is a critical regulator of autophagy induction; activated mTOR suppresses autophagy, whereas negative regulation of mTOR promotes it [21]. For this reason, we tested if mTOR activation is deregulated in mutated cells. We have found that in starving conditions and without SCF, cells carrying the D816V mutation have increased phosphorylation of mTOR and its downstream effector 4E-BP1. Moreover, stimulation with SCF increases phosphorylation of the mTOR pathway (Figure 4F). These results suggest

that KIT WT cells need SCF to activate the mTOR pathway, whereas this pathway is constitutively activated in mutated cells.

BNIIP3 expression in AML patients with *the* KIT D816V mutation

We performed a Bloodspot analysis (www.bloodspot.eu) of BNIP3 in normal and AML samples to study BNIP3 expression. We found that the BNIP3 level in AML patients with t(8;21) and inv (16) was lower than in other AML subtypes (Figure 5A). Interestingly, mutations of KIT occur in 20–25% and approximately 30% of AML t(8;21) and inv(16) cases, respectively (22). We checked the BNIP3 influence on overall survival in the TGGA AML cohort and detected a decreased survival probability in patients with BNIP3 downregulation (Supplementary Figure 4). Given these results, we analyzed BNIP3 expression in AML patients with t(8;21) or inv (16). First, we assessed the presence of the KIT D816V mutation, and we measured BNIP3 expression by RT-qPCR in patients with or without this mutation. As expected, BNIP3 expression was significantly decreased in patients carrying the KIT D816V mutation (Figure 5B).

DISCUSSION

In the current study, we found that, compared to KIT WT, mutated KIT D816V cell lines ROSA and TF-1 significantly increased mitochondrial activity and number. Consequently, we detected more superoxide production, which could increase DNA instability. The most frequent pathogenic driver of systemic mastocytosis. (SM) is the KIT D816V mutation. Early acquisition of this mutation during hematopoiesis may result in multilineage involvement by KIT D816V. This has been linked to an increased incidence of transition to advanced SM [23].

Linked to these findings, we found a decreased expression of BNIP3 in KIT mutant cell lines, a protein that regulates apoptosis and autophagy [24], and LC3, resulting in reduced autophagy. These results could explain the increased mitochondrial number found. We revert the mitochondrial number by overexpressing BNIP3, resulting in an increase in autophagy through LC3 lipidation. Finally, we confirmed by RT-qPCR that AML patients carrying *the KIT* D816V mutation had decreased BNIP3 levels.

mTOR activation is active only when nutrients and growth signals are present [25]. We observed that mutated KIT cells have the mTOR pathway active constitutively in starving conditions, not depending on the viability of cytokines, resulting in unrestricted growth, a hallmark of cancer. mTOR is hyperactivated in up to 80% of cancers [26]

The KIT D816V mutation reduces cellular dependence on extrinsic signals (a hallmark of cancer) to maintain survival, growth, and proliferation that, in normal conditions, are under the control of cytokines [7]. Loss of this growth factor dependence allows cells to maintain signal transduction pathways, and cellular metabolism needs to be rewired to sustain this hyperactivated state. We found increased mitochondrial activity and ATP production caused by mitochondrial changes, suggesting that mitochondrial metabolism is not intrinsically impaired in KIT D816V cells. This phenomenon is opposite to the Warburg effect, which describes a glycolytic upregulation in cancer cells characterized by high glucose consumption and lactate production even in oxygen [19,20]. It has been described that mitochondrial metabolism is not impaired, as in our models, in some cancers such as leukemias, lymphomas, pancreatic ductal adenocarcinoma, a subgroup with high OXPHOS melanomas, and endometrial carcinoma [27,28].

Our findings align with earlier studies in AML cells that show a greater copy number of mtDNA compared to normal HSCs [29]. Chronic lymphocytic leukemia (CLL) also has increased mitochondrial mass [30], and it has been shown that the stromal environment increases OXPHOS in CLL [31]. These results suggest an increased OXPHOS in hematologic neoplasms and may indicate that the microenvironment strongly influences metabolism in blood neoplasms. However, each type of leukemia may behave in a specific way. Isocitrate dehydrogenase (IDH) or FLT3 mutations have been associated with glycolysis upregulation [32-34].

Alterations in intracellular levels of ROS have been associated with changes in mitochondrial abundance, mtDNA copy number, and the expression of respiratory genes [35]. ROS are produced during normal cellular metabolic processes, and mitochondria are the main source of their production. An imbalance between the production and scavenging of ROS will damage cellular proteins, lipids, and nucleic acids [35]. We showed an increase in superoxide production in ROSA and TF-1 KIT D816V cell lines and an increased 8-OHdG level in ROSA mutant cells, a biomarker of oxidative damage to DNA. 8-OHdG residues in DNA result in a GC to TA transversion, which may cause damage to DNA replication [36]. Accordingly, 8-OHdG in cells may lead to mutagenesis and thus play a significant role in cancer evolution. Increased levels of ROS have been associated with a high rate of

mutations [37]. We cannot rule out that successive mutations acquired after *KIT* D816V could change the metabolic profile, switching cells to a mainly glycolytic phenotype [38].

We found that increased mitochondrial number is a consequence of reduced mitophagy in mutated KIT D816V cell lines due to BNIP3 down-regulation, and we showed that BNIP3 expression might be critical for mitochondrial number. Several studies have demonstrated that BNIP3 is a potent inducer of autophagy [24,39,40]. Rikka et al. [41] showed that BNIP3 overexpression led to the loss of Δψm, diminished the capacity to produce ATP, and impaired mitochondrial respiration. Glick et al. [42] showed that BNIP3 hepatocytes from BNIP3-null mice had an increased number of mitochondria, and these mitochondria were also smaller when compared to those from BNIP3 WT mice. These results are clearly in line with our findings, linking BNIP3 expression with mitochondrial morphology and number.

BNIP3 deregulation has been previously described in various cancer types. In solid tumors, BNIP3 is induced under hypoxic conditions [43], overexpressed at premalignant stages, and downregulated upon progression to more invasive and aggressive forms [44,45,46]. On the other hand, lower BNIP3 expression has been observed in cell lines and primary tumor cells. Down-regulation of BNIP3 has been associated with a chemo-resistant phenotype and a bad outcome [47]. Thus, in some stages of tumorigenesis, decreased mitophagy may allow for a permissive threshold of dysfunctional mitochondria to persist, generating increased tumor-promoting ROS. Established cancers may require mitophagy for stress adaptation and survival [48]. BNIP3 could be downregulated in hematologic malignancies by different mechanisms [49,50]. Interestingly, BNIP3, when dimerized, is inserted into the mitochondrial membrane, and it induces cell death through apoptotic, necrotic, and autophagic pathways [47]. Decreased BNIP3 expression could also be a means of avoiding cell death in KIT D816V cells, and its downregulation could be a survival mechanism.

Materials and methods

Oxygen Consumption Rate

Oxygen Consumption Rate (OCR) was performed using the XF24e Extracellular Flux Analyzer following the manufacturer's instructions and using the materials provided (Seahorse Bioscience, Billerica, MA). Cells were immobilized using Cell-Tak (Corning, NY, USA) in 24- well culture plate and seeded at $5x10^5$ cells/well for the ROSA cell line and $1x10^5$ cells/well for the TF-1 cell line. Cells were equilibrated for 1 hour in XF seahorse base medium supplemented with 1 mM sodium pyruvate, 2 mM L-glutamine, and 5 mM glucose at

37°C in CO_2 free incubator before the seahorse experiment. Oligomycin was added at 1 µM and CCCP at 0.5 for ROSA and 1 µM for TF-1 cells into the seahorse medium.

ATP quantification

Cellular ATP content was measured using the ATP determination kit (Life Technologies Europe, Netherlands). One hundred thousand cells were washed in ice-cold PBS, pelleted, resuspended in ATP buffer (100 mM Tris-HCl pH 7.75, 4 mM EDTA), frozen in liquid nitrogen, and boiled for 3 minutes. Cells were placed on ice for 5 minutes and centrifuged at 13.000 rpm for 5 min at 4ºC. The supernatant was recovered, and ATP levels were measured using the manufacturer's protocol. Luminescence was calculated using the luminometer Lumat LB Tube (Berthold Technology, Germany)

Mitochondrial oxidative damage

Cells were seeded into wells with poly-L-lysine-coated cover glasses (Sigma-Aldrich) and incubated for 1 hour at 37°C in 5% CO2. Cells were fixed in 4% PFA for 10 min and permeabilized with 0.5% Triton in PBS for 10 min. The wells were washed twice in PBS and blocked with PBS containing 1% BSA for 1 hour at room temperature. The Anti-8 Hydroxyguanosine antibody recognized oxidized nucleotides (Abcam) used at 1:500 for 1 hour at room temperature, followed by incubation with Goat Anti-Mouse IgG H&L Alexa Fluor® 647 (Abcam) used at 1:200 for 1 hour at room temperature. Nuclei were counterstained with DAPI (Molecular Probes, Life Technologies, Paisley, Scotland) at 300 nM for 3 minutes. Samples were observed using a Confocal multispectral Leica SP5 microscope (Wetzlar, Germany). The experiment was performed in triplicate, and several images were captured.

BNIP3 expression in AML patients

Primary samples from AML patients have obtained from the Department of Hematology at the Hospital de la Santa Creu I Sant Pau in Barcelona (Catalonia, Spain) with full informed consent from the patients and the approval of the corresponding Institutional Review Boards.

RNA obtained from 34 patients diagnosed with AML1-ETO and 38 with CBFB-MYH11 were tested for KIT D816V mutation as described previously [52]. The probes for the BNIP3 (Hs00969291_m1) and ABL1 (Hs01104728_m1) were purchased as Assay-on-Demand (Applied Biosystems). Gene expression data were analyzed by the ΔΔCt method, using *ABL*1 as an internal control.

Statistical methods

Statistical analysis was performed using GraphPad Prism version 5.0 software (GraphPad, CA, USA) Graphs represent three independent experiments and results were normalized by KIT WT cells. All values were expressed as the means ± standard error of the mean (S.E.M) and statistical significance was determined using the Student t-test. A value of $p < 0.05$ was regarded as significant: *, **, and *** correspond to $p < 0.05$, $p < 0.01$, and $p < 0.001$, respectively.

Additional methods are available at the Supplementary section.

Acknowledgments

The following grants supported this work: PI13/2729 and PI16/094 from the Instituto de Salud Carlos III, Ministerio de Economía y Competitividad, Spain; 2014-SGR-383, 2017-SGR-1395 and PERIS SLT 002/16/0043 from Plà de Recerca de Catalunya.

The authors also thank Aix-Marseille University and the Amidex Foundation for providing funds to support fundamental research. This study was also in part supported by research funding from the Canceropôle Provence-Alpes-Côte d'Azur, the French National Cancer Institute (INCa) and the Provence-Alpes-Côtes d'Azur Region.

Authorship contributions

Study conception and design: SC-W, AZ, and JN

Acquisition, analysis and interpretation of data: SC-W, MIHA, EB, AZ and JN.

Drafting of the manuscript: SC-W and JN

Critical revision: All authors

Competing interests statement

The authors declare no competing interests.

References

1. Chen, S.Q., Xiong, A.Q. The progress and implication of stem cell factor. *Basic Med. Sci*.; 22, 385–390 (2002).
2. Valent, P., Akin C, Hartmann K., Nilsson, G., Reiter ,A., et al. Advances in the classification and treatment of mastocytosis: Current status and outlook toward the future. *Cancer Res*.; 77, 1261–1270 (2017).
3. Beghini, A., Ripamonti, C.B., Cairoli, R., Cazzaniga, G., Colapietro, P., Elice, F., et al. KIT activating mutations: Incidence in adult and pediatric acute myeloid leukemia, and identification of an internal tandem duplication. *Haematologica;* 89, 920–925 (2004).
4. Corless, C.L., Fletcher, J.A., Heinrich, M.C. Biology of gastrointestinal stromal tumors. *J Clin. Oncol;* 22, 3813–3825 (2004).
5. Curtin, J.A., Busam K., Pinkel D., Bastian B.C. Somatic activation of KIT in distinct subtypes of melanoma. *J Clin. Oncol;* 24, 4340–4346 (2006).
6. Tian, Q., Frierson, H.F., Krystal, G.W., Moskaluk, C.A. Activating c-kit gene mutations in human germ cell tumors. *Am. J. Pathol;* 154, 1643–1647 (1999).
7. Furitsu, T, Tsujimura, T,, Tono, T., Ikeda, H., Kitayama, H. Identification of Mutations in the Coding Sequence of the Proto-oncogene c-kit in a Human Mast Cell Leukemia Cell Line Causing Ligand-independent Activation of c-kit Product. *J. Clinical Invest*.; 92, 1736-1744 (1993).
8. Kitayama, H., Tsujimura, T., Matsumura, I., Oritani, K., Ikeda, H., et al. Neoplastic transformation of normal hematopoietic cells by constitutively activating mutations of c-kit receptor tyrosine kinase. *Blood;* 88, 995–1004 (1996).
9. Ashman, L.K.M, Griffith, R. Therapeutic targeting of c-KIT in cancer. Expert. *Opin. Investig. Drugs;* 22, 103–115 (2013).
10. Hanahan, D., Weinberg, R.A., Hallmarks of cancer: the next generation. *Cell*; 144, 646–674 (2011).
11. Nagarajan, A., Malvi, P., Wajapeyee, N. Oncogene-directed alterations in cancer cell metabolism. *Trends Cancer;* 2, 365–377 (2016).
12. Kitamura, T., Tange, T., Terasawa, T., Chiba, S., Kuwasaki, T., Miyagawa, K., et al. Establishment and characterization of a unique human cell line that proliferates dependently on GM-CSF, IL-3, or erythropoietin. *Cell Physiol;* 140, 323-334 (1989).

13. Saleh, R., Wedeh, G., Herrmann, H., Bibi, S., Cerny-Reiterer, S., et al. A new human mast cell line expressing a functional IgE receptor converts to tumorigenic growth by KIT D816V transfection. *Myeloid neoplasia;* 124, 111–121 (2019).
14. Sriskanthadevan, S., Jeyaraju, D. v., Chung, T. E., Prabha, S., Xu, W., Skrtic, M., et al. AML cells have low spare reserve capacity in their respiratory chain that renders them susceptible to oxidative metabolic stress. *Blood*; *125*-13 (2015).
15. Zhang, B., Alysandratos, KD., Angelidou, A., et al. Human mast cell degranulation and preformed TNF secretion require mitochondrial translocation to exocytosis sites: relevance to atopic dermatitis. *J. Allergy Clin. Immunol*.; 127, 1522-31 (2011).
16. Warburg, O. On the origin of cancer cells. *Science;* 123, 309–314 (1956).
17. Hsu P.P., Sabatini, D.M. Cancer cell metabolism: Warburg and beyond. *Cell;* 134, 703–707 (2008).
18. Turrens, J.F. Mitochondrial formation of reactive oxygen species. *J. Physiol*.; 552, 335–344 (2003).
19. Pickles, Sarah, Pierre Vigié, y Richard J. Youle. Mitophagy and Quality Control Mechanisms in Mitochondrial Maintenance. *Current Biology;* 28, 170-85 (2018)
20. Kubli D, Gustafsson Å. Mitochondria and mitophagy: the yin and yang of cell death control. *Circ Res*; 111, 1208–1221 (2012).
21. Laplante, M., & Sabatini, D. M. mTOR Signaling in Growth Control and Disease. *Cell*; *149*, 274–293 (2012).
22. Ayatollahi H, Shajiei A, Sadeghian MH, et al. Prognostic Importance of C-KIT Mutations in Core Binding Factor Acute Myeloid Leukemia: A Systematic Review. *Hematol Oncol Stem Cell Ther*.; 101, 1-7 (2017).
23. Papaemmanuil, E, Gerstung, M, Malcovati L. Tauro S. et al. Clinical and biological implications of driver mutations in myelodysplastic syndromes. Blood; 122, 3616–3627 (2013).
24. Zhang, J., Ney, P. A., Role of BNIP3 and NIX in cell death, autophagy, and mitophagy. *Cell Death Differ.;* 16, 939–946 (2009)
25. Laplante M, Sabatini DM. mTOR Signaling in Growth Control and Disease. *Cell*; 149, 274–293 (2012).

26. Liu G.Y., Sabatini D.M. mTOR at the Nexus of Nutrition, Growth, Ageing and Disease. Nat. Rev. Mol. Cell Biol.; 21,183–203 (2020)
27. Weinberg, S., Chandel, N. Targeting mitochondria metabolism for cancer therapy. *Nat Chem Biol*; 11, 9–15 (2015).
28. Moreno-Sanchez, R., Rodriguez-Enriquez, S., Marin-Hernandez, A., Saavedra, E. Energy metabolism in tumor cells. *FEBS J*.; 274, 1393–418 (2007).
29. Škrtić, M., Sriskanthadevan, S., Jhas, B., Gebbia, M., Wang, X., et al. Inhibition of Mitochondrial Translation as a Therapeutic Strategy for Human Acute Myeloid Leukemia. *Cancer Cell*; 20, 674–88 (2011).
30. Chowdhury, S.R., Banerji, V. Targeting Mitochondrial Bioenergetics as a Therapeutic Strategy for Chronic Lymphocytic Leukemia. *Oxid. Med. Cell Longev*.; 28, 242671224 (2018)
31. Vangapandu, H.V., Ayres, M.L,: Bristow, C.A., Wierda, W.G., Keating, M.J., et al. The Stromal Microenvironment Modulates Mitochondrial Oxidative Phosphorylation in Chronic Lymphocytic Leukemia Cells. *Neoplasia*; 19, 762–771 (2017).
32. Ju, H.Q., Zhan, G., Huang, A., Sun, Y., Wen, S., et al. ITD mutation in FLT3 tyrosine kinase promotes Warburg effect and renders therapeutic sensitivity to glycolytic inhibition. *Leukemia*; 31, 2143–2150 (2017).
33. Fujiwara, H., Tateishi, K., Misumi, K., Hayashi, A., Igarashi, K., et al. Mutant IDH1 confers resistance to energy stress in normal biliary cells through PFKP-induced aerobic glycolysis and AMPK activation. *Sci. Rep*.; 9, 2045-2322 (2019).
34. Ju, H. Q., Zhan, G., Huang, A., Sun, Y., Wen, S., et al. ITD mutation in FLT3 tyrosine kinase promotes Warburg effect and renders therapeutic sensitivity to glycolytic inhibition. *Leukemia*; 31, 2143–2150 (2017).
35. Lee, H.C., Wei, Y.H. Mitochondrial biogenesis and mitochondrial DNA maintenance of mammalian cells under oxidative stress. *Int J Biochem Cell Biol*.; 37, 822–834 (2005).
36. Breen, A.P., Murphy, J.A. Reactions of oxyl radicals with DNA. *Free Radic. Biol. Med*.; 18, 1033-1077 (1995).

37. Cheng, K.C., Cahil,l D.S., Kasai, H., Nishimura, S. 8-Hydroxyguanine, an abundant form of oxidative DNA damage, causes G→T and C→A substitutions. *J Biol Chem*.; 267, 166–72 (1992).
38. Waris, G., Ahsan, H. Reactive oxygen species: Role in the development of cancer and various chronic conditions. *J Carcinog.;* 5, 1–8 (2006).
39. Quinsay, M.N., Thomas, R.L., Lee, Y., Gustafsson, A.B., Bnip3-mediated mitochondrial autophagy is independent of the mitochondrial permeability transition pore. *Autophagy.;* 6, 17–24 (2010).
40. Bellot, G., Garcia-Medina, R., Gounon, P., Chiche, J., Roux, D., Pouyssegur, J., et al. Hypoxia- induced autophagy is mediated through hypoxia-inducible factor induction of BNIP3 and BNIP3L via their BH3 domains. *Mol Cell Biol*.; 29, 2570–2581 (2009).
41. Rikka, S., Quinsay, M.N, Thomas, L.R., Kubli D.A., Zhang, X., et al. Bnip3 impairs mitochondrial bioenergetics and stimulates mitochondrial turnover. *Cell Death Differ*.; 18, 721–731 (2011).
42. Glick, D., Zhang, W., Beaton, M., Marsboom, G., Gruber, M., et al. BNip3 Regulates Mitochondrial Function and Lipid Metabolism in the Liver. *Mol Cell Biol*.; 32, 2570–2584 (2012).
43. Guo, K., Searfoss,G., Krolikowski ,G., Pagnoni, M., Franks, C., et al. Hypoxia induce the expression of the pro-apoptotic gene BNIP3. *Cell Death Differ*.; 83 67–376 (2001).
44. Sowter, H.M., Ferguson, M., Pym, C., Watson, P., Fox, S.B., et al. Expression of the cell death genes BNip3 and Nix in ductal carcinoma in situ of the breast. correlation of BNip3 levels with necrosis and grade. *J Path*.; 201, 573–80 (2003).
45. Koop, E.A., van Laar, T., van Wichen, D.F., de Weger, R.A., van der Wall, E., van Diest, P.J., Expression of BNIP3 in invasive breast cancer: correlations with the hypoxic response and clinicopathological features. *BMC Cancer*; 175, 2157-9024 (2009).
46. Erkan, M., Kleef, J., Esposito, I., Giese, T., Ketterer, K., et al. Loss of BNIP3 expression is a late event in pancreatic cancer contributing to chemoresistance and worsened prognosis. *Oncogene*; 24, 4421–32 (2005).
47. Burton, T.R., Gibson, S.B. The role of Bcl-2 family member BNIP3 in cell death and disease. *Cell Death Differ*.; 16, 515-523 (2009).

48. Vyas, S., Zaganjor, E., Haigis, M.C.Mitochondria and Cancer. *Cell*.; 166, 555–566 (2016).
49. Lazarini, M., Machado-Neto, J., Duarte, A. S., Pericole, F. V., Favaro, P., Barcellos, K., et al. BNIP3 Is Downregulated in Myelodysplastic Syndromes and Acute Myeloid Leukemia and Is a Potential Molecular Target for Decitabine. *Blood*; 120, 0006-4971 (2012).
50. Murai, M., Toyota, M, Satoh, A., Suzuki, H., Akino, K., et al. Aberrant DNA methylation associated with silencing BNIP3 gene expression in haematopoietic tumours. *Br J Cancer*; 92, 1165–1172 (2005).

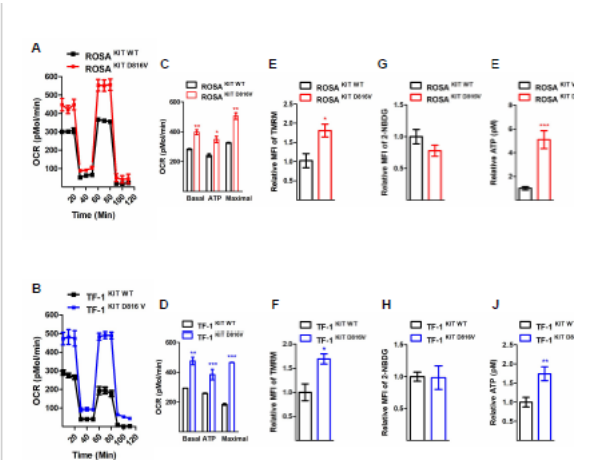

Figure 1. Increased respiratory rates and respiratory capacity in KIT D816V cells.

Seahorse XF24 assay as represented by continuous measurements of oxygen consumption (OCR) of ROSA (**A**) and TF-1 cells (**B**) in basal conditions and after sequential addition of Oligomycin, CCCP, and Rotenone/Antimycin. Continuous OCR values (pMols/min) are shown for one representative of three experiments. Basal Respiration, ATP-linked respiration, and maximal respiratory capacity in ROSA and TF-1 cells were calculated (**C, D**). Mitochondrial membrane potential using tetramethylrhodamine methyl ester (**E, F)** and glucose uptake using the 2-NBDG tracer (**G, H**) were measured by flow cytometry in ROSA and TF-1 cell lines. The values show the median fluorescence intensity (MFI) of three independent experiments normalized by KIT WT cells. ATP concentration was measured by bioluminescence in ROSA and TF-1 cells (**I, J**) using the luciferase-coupled ATP determination kit. The values show the median of four independent experiments normalized by KIT WT cells. Data are mean ± SEM. *p≤0.05, **p≤0.005, ***p≤0.001 vs. wild-type group.

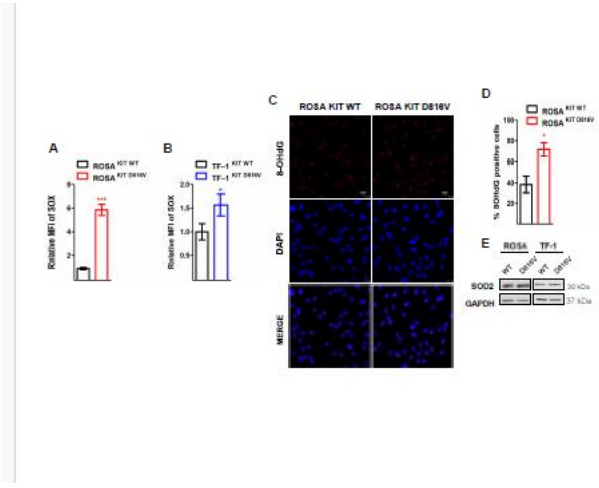

Figure 2. Increased superoxide production in KIT D816V cells

Superoxide production was measured by flow cytometry using MitoSOX reagent in ROSA (**A**) and TF-1 (**B**) cell lines. The values show the median fluorescence intensity (MFI) of three independent experiments normalized by KIT WT cells. Oxidative damage was measured in ROSA cells (**C**) by immunofluorescence of 8-hydroxydeoxyguanosine (8-OHdG) as a marker (red). The nucleus was identified with DAPI (blue). One representative image is shown of three independent experiments. Scale bars represent 10 µm. (**D**) 8-OHdG fluorescence was quantified using ImageJ software. (**E**) Immunoblotting of Superoxide Dismutase 2 (SOD2) in ROSA and TF-1 cell lines. One representative image of three experiments is shown. Data are mean ± SEM. *p≤0.05, **p≤0.005, ***p≤0.001 vs. wild-type group.

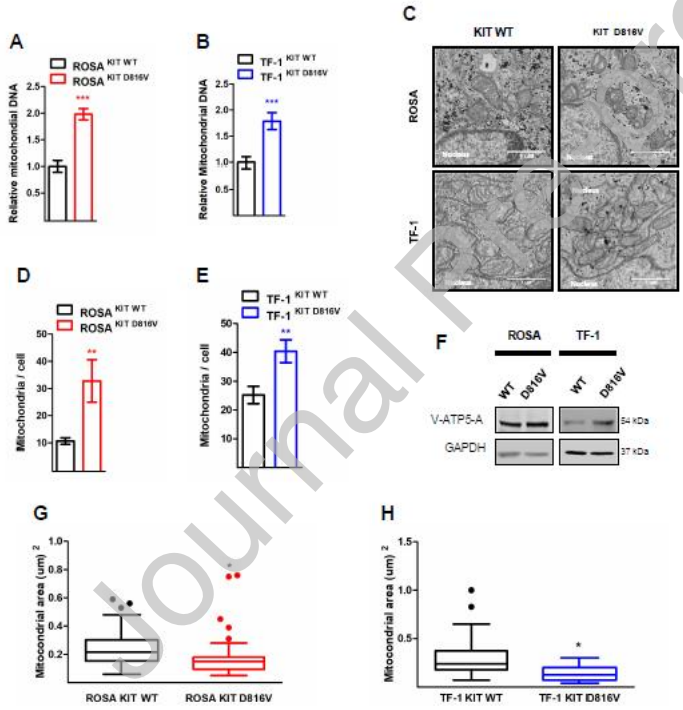

Figure 3. Mitochondrial quantification

Relative mitochondrial content (mtDNA) was measured by Q-PCR in ROSA (**A**) and TF-1 (**B**) cell lines by determining the ratio between the mitochondrial sequence COX2 and the nuclear sequence β-actin. The graph represents the media of three independent experiments. The results are normalized by WT cells. (**C**) Representative mitochondrial images of ROSA and TF-1 KIT WT and D816V cell lines. Scale bars represent 1 µm. Using

ImageJ software, the mitochondria number per cell was counted from TEM aleatory images in ROSA (**D**) and TF-1 cells (**E**). (**F**) Immunoblotting of mitochondrial respiratory subunit alpha of complex V (ATP synthase or ATPase). One representative experiment of three is shown. The mitochondrial area of ROSA (**G**) and TF-1 (**H**) cells was measured using ImageJ software. One representative image of three experiments is shown. Data are mean ± SEM. *p≤0.05, **p≤0.005, ***p≤0.001 vs. wild-type group.

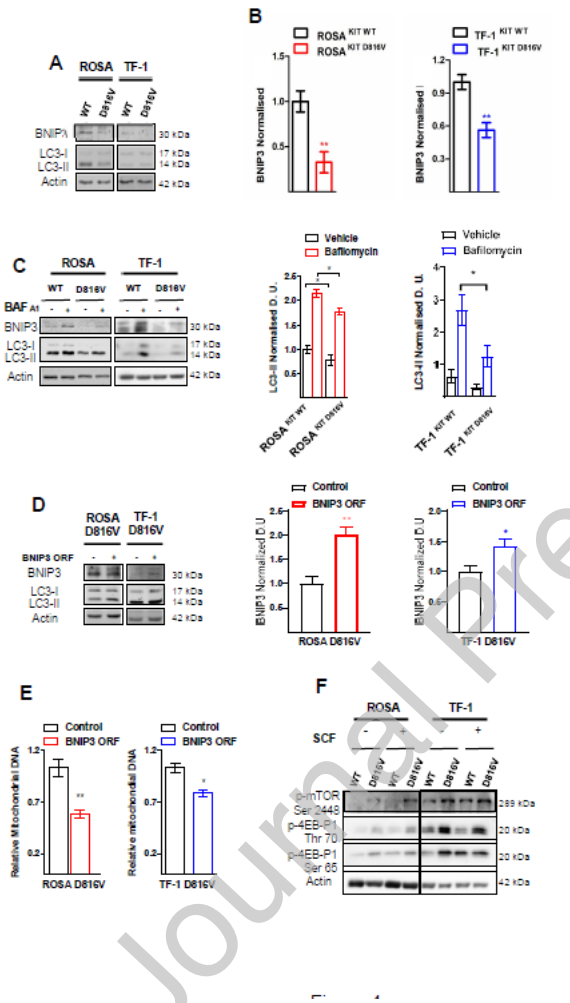

Figure 4. Mitochondrial biogenesis and mitophagy in KIT mutated cell lines.

(**A**). Immunoblotting of autophagic markers BNIP3 and LC3 in ROSA and TF-1 cell lines. (**B**) BNIP3 mRNA expression was measured in ROSA and TF-1 cells by Q-PCR. ABL1 was used as internal control. (**C)** Immunoblotting of BNIP3 and LC3 of ROSA and TF-1 cells incubated with Bafilomycin A1 (Baf A1) at 100 nM for 6 h for ROSA cells and 130 nM for 7 h for TF-1 cells or vehicle to inhibit autophagosome degradation. (**D**) Immunoblotting of BNIP3 and LC3 of mutated ROSA and TF-1 cells lines were infected with an adenoviral vector encoding BNIP3. (**E**) Relative mitochondrial content was measured in ROSA and TF-1 mutated cell lines infected with ORF BNIP3 by Q-PCR. Actin was used as internal control, (**F**) mTOR

markers were measured by immunoblotting without and after SCF activation. Graphs represent the media of three independent experiments. The results are normalized by WT or control cells. Westerns blots are performed by triplicate, and one representative image is showed. Immunoblotting graphs represent the median of three independent experiments and are normalized by actin. Data are mean ± SEM. *p≤0.05, **p≤0.005, ***p≤0.001 vs. wild-type group.

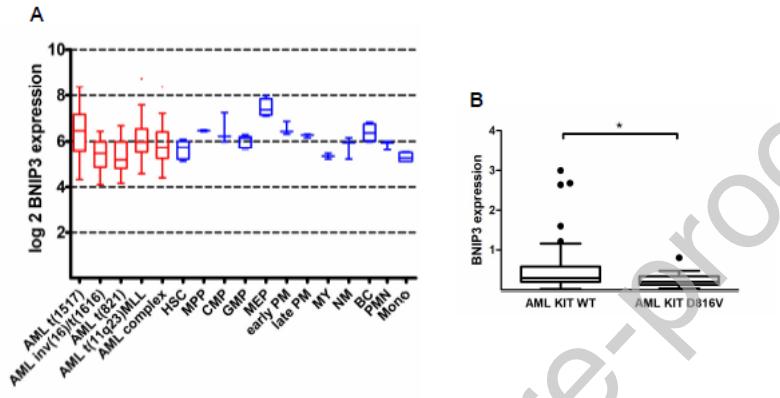

Figure 5. BNIIP3 expression in AML patients with the KIT D816V mutation.

(A) Bloodspot analysis of BNIP3 in normal hematopoiesis and AML. (**B**) BNIP3 expression was measured in 34 AML patients with t(8;21) or inv(16) by RT-qPCR with KIT WT or KIT D816V mutation. *p≤0.05

Graphical abstract